JOURNAL OF GEOPHYSICAL RESEARCH: OCEANS, VOL. 118, 6371–6384, doi:10.1002/2013JC009243, 2013

Sea surface transport in the Western Mediterranean Sea: A Lagrangian perspective

J.-M. Sayol,[1] A. Orfila,[1] G. Simarro,[2] C. López,[3] L. Renault,[4] A. Galán,[5] and D. Conti[1]

Received 28 June 2013; revised 31 October 2013; accepted 31 October 2013; published 2 December 2013.

[2] We study the sea surface transport in the Western Mediterranean Sea from a Lagrangian point of view, in particular the Alboran and the North-Western subbasins. The study is carried out through the analysis of 3 years of surface velocity model data through Finite Size Lyapunov Exponents, Residence Time, and virtual particle trajectories complementing the classical Eulerian approach. The spatiotemporal variability of the main transport processes is inferred from the Empirical Orthogonal Function modes of the Lyapunov Exponents, being the most relevant modes discussed and physically interpreted. Results indicate that some of the variability in the surface transport patterns in the Western Mediterranean can be explained by specific modes which provide an indication of connectivity among subbasins, like the inflow of Atlantic waters through the Ibiza Channel.

Citation: Sayol, J.-M., A. Orfila, G. Simarro, C. López, L. Renault, A. Galán, and D. Conti (2013), Sea surface transport in the Western Mediterranean Sea: A Lagrangian perspective, *J. Geophys. Res. Oceans*, *118*, 6371–6384, doi:10.1002/2013JC009243.

1. Introduction

[3] The Western Mediterranean Sea (WMS) is a marine biodiversity hot spot, a place where coexist physical processes at different spatial and temporal scales interacting among them [*Roussenov et al*., 1995; *Bergamasco and Malanotte-Rizzoli*, 2010]. The circulation of the surface waters in the WMS is the result of the energetic inputs, mainly from wind at the most surface layers, and the interaction of water masses of different densities—see *Millot* [1999] for a complete description of the general circulation in the WMS. Surface waters are formed by water masses with different characteristics; the "new" Atlantic Water (AW) that are fresh waters of recent origin with low salinity (about 36.5 psu) that entered into the basin through the Strait of Gibraltar, mix with older and saltier waters (above 38 psu) coming from the North-Western subbasin. The study of these interactions is an active research area since it is a key element to understand the general circulation, as well as the (sub)mesoscale dynamics modulating the biological response around the area.

[4] A better insight of ocean circulation has been possible, in part, thanks to improvements in the Lagrangian observational techniques [*Poulain et al*., 2012], as well as by the development of a theoretical basis for the Lagrangian characterization or, in other words, the study of ocean flows by following fluid particle trajectories [*Mariano et al*., 2002; *d'Ovidio et al*., 2004; *Shadden et al*., 2005; *Mancho et al*., 2006]. The transport in the ocean surface has been thus approached under this Lagrangian perspective [*Buffoni et al*., 1997; *Özgökmen et al*. 2000; *Iudicone et al*., 2002; *Molcard et al*., 2006; *d'Ovidio et al*., 2009], providing additional information on the mixing properties of the ocean surface, with practical applications in physics and biology, such as the study of the fate of pollutants [*Lekien et al*., 2005; *Olascoaga and Haller*, 2012], the determination of the paths of chlorophyll [*Lehahn et al*., 2011] or the study of the dispersion and mixing of coastal waters [*Haza et al*., 2010; *Galán et al*., 2012].

[5] A relevant Lagrangian technique widely used in oceanographic studies is that of Finite-Size Lyapunov Exponents (FSLE) [*Artale et al*., 1997; *Aurell et al*., 1997]. FSLE measures the local dispersion and also serves for identifying Lagrangian Coherent Structures (LCS) like vortices, barriers to transport and filaments organizing the fluid flow [*Haller and Yuan*, 2000; *Boffetta et al*., 2001; *Lapeyre*, 2002; *Joseph and Legras*, 2002; *d'Ovidio et al*., 2004; *Tew Kai et al*., 2009]. Thus, FSLE fields allow to identify regions of locally maximum compression, approximating attracting or unstable manifolds of hyperbolic trajectories, which can be identified with the LCS. Attracting LCS associated to backward integration has a direct physical interpretation. In this work, we use the FSLE for the characterization of dispersion and mixing processes in the marine surface.

[6] We analyze 3 years of data, from 1 February 2009 to 31 January 2012 of the dynamics of surface circulation of the WMS, as well as the paths of connectivity between two subbasins: the Alboran Sea and the North-Western (which

Additional supporting information may be found in the online version of this article.

[1]IMEDEA(CSIC-UIB), Esporles, Balearic Islands, Spain.
[2]ICM-CSIC, Barcelona, Spain.
[3]IFISC(CSIC-UIB), Palma, Balearic Islands, Spain.
[4]ICTS SOCIB, 07121, Palma, Balearic Islands, Spain.
[5]E.T.S.I. de Caminos, Canales y Puertos, UCLM, Ciudad Real, Spain.

Corresponding author: J.-M. Sayol, Institut Mediterrani d'Estudis Avançats (CSIC-UIB), C/Miquel Marques 21, Esporles, 07190 Balearic Islands, Spain. (jsayol@imedea.uib-csic.es)

2169-9275/13/10.1002/2013JC009243

includes the Catalan Sea and the Gulf of Lions) subbasins. The starting point is the data provided by a realistic eddy resolving three-dimensional numerical model. In this work, we use the Lagrangian approach to get a complete picture of the spatiotemporal surface circulation of the WMS. Masses of water are tracked trying to understand their spatial patterns as well as their variability at a seasonal scale. To do that, the most relevant patterns of variability in FSLE fields are decomposed using Empirical Orthogonal Functions (EOFs) [*Emery and Thomson*, 2004]. Connectivity between the Alboran Sea and the North-Western subbasins is done by tracking the surface waters crossing the Ibiza Channel, a key place for north-south exchange which has been already identified as a choke point for the biogeochemistry transport.

[7] This work is organized as follows. In section 2, we describe the area of study depicting its main characteristics. In section 3, the numerical model data and computational methods are presented. In section 4, a statistical characterization of the FSLE is carried out through an EOF decomposition. Significant modes for the Alboran Sea and the North-Western subbasins are physically interpreted and the connection between both through the Ibiza Channel outlined. The analysis is complemented by the computation of the Residence Time in the two subbasins. Section 5 concludes the work and outlines some future research lines.

2. Area of Study

[8] The WMS surface circulation is mainly driven by the intrusion of AW across the Strait of Gibraltar and by the wind forcing at the ocean surface [*André et al.*, 2005]. In the North-Western subbasin (top dashed box in Figure 1a), the circulation is characterized by the presence of the Northern Current (NC) flowing southwestward along the continental slope until exiting the basin through the Ibiza Channel (Figure 1b, down dashed box). Some of these waters are retroflected cyclonically to form, along with the

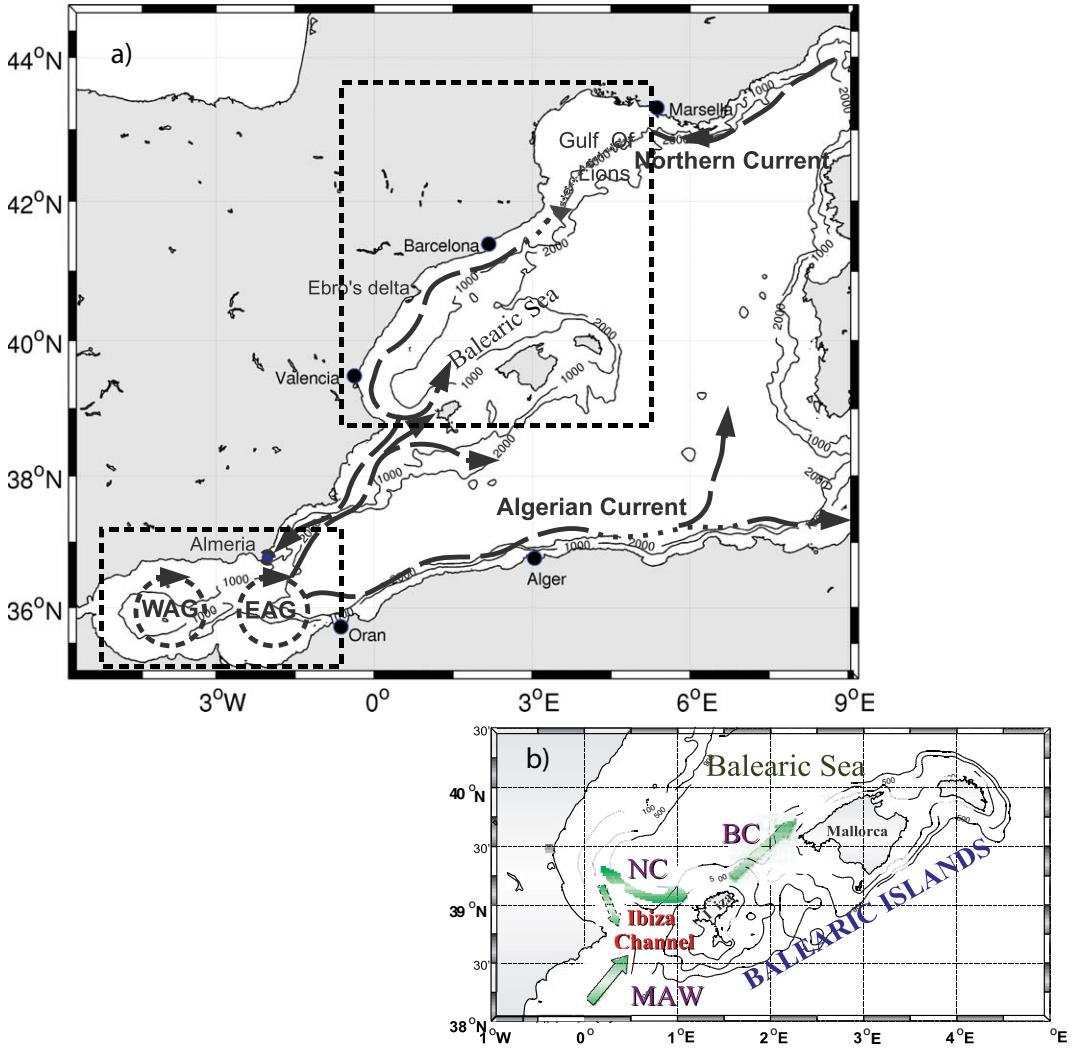

Figure 1. (a) Geographical location of the study area where the main currents are outlined. WAG (Western Alboran Gyre); EAG (Eastern Alboran Gyre); AC (Algerian Current); NC (Northern Current); BC (Balearic Current); and AW (Atlantic Water). Dashed rectangles indicate the subbasins the Alboran Sea and the North-Western area. (b) Sketch of the main currents across the Ibiza Channel.

inflow of AW, the Balearic Current (BC) [*Font et al*., 1988]. Observations of the seasonal frequency of the NC show higher transport in winter than in summer (1.5–2 Sv and 1 Sv, respectively), while the opposite is found in the BC (0.3 Sv in winter compared with 0.6 Sv in summer) [*Font et al*., 1995; *Pinot et al*., 2002]. The intensity as well as the causes of this variability are still open questions. Southward transport is believed to be controlled by an eddy blocking often associated with cold cores of Western Mediterranean Intermediate Water [*Heslop et al*., 2012]. Besides, the inflow of AW is likely controlled by the weakening of the NC and/or by the mesoscale activity in the southern side of the Balearic Islands [*Pinot et al*., 2002].

[9] This general pattern forms the Catalan front that separates the saltier "old" AW found in the central part of the Balearic Sea from fresher waters on the Catalan shelf. The Balearic subbasin is governed by an intense frontal dynamical zone on the shelf-slope area as the result of the interaction between the BC and the NC that results on the generation of mesoscale eddies, filaments, and intense shelf-slope interactions [*Wang et al*., 1988; *La Violette et al*., 1990; *Rubio et al*., 2009].

[10] Regarding the surface inputs, the Gulf of Lions and the Balearic Sea are characterized by the influence of the Mistral and Tramontane winds (both from the northern sector) [*Jansà*, 1987]. These winds frequently extend several hundreds of kilometers from the coast carrying cold and dry continental air over the warmer ocean surface and, producing as a result, an intense heat exchange between the ocean and the atmosphere with the subsequent sea surface cooling [*Estournel et al*., 2003; *Renault et al*. 2012a].

[11] The Alboran subbasin extends from the Strait of Gibraltar, at the west, to Oran, at the east. It presents a characteristic circulation given by the existence of a quasi-permanent anticyclonic eddy, the Western Alboran Gyre (WAG) with a typical diameter of 100–150 km, and a more variable anticyclonic gyre at the east, the Eastern Alboran Gyre (EAG). According to *Viúdez et al*. [1996, 1998], *Vargas-Yáñez et al*. [2002], and *Renault et al*. [2012b] a two gyres-circulation regime (WAG + EAG) prevails during summer, while a single anticyclonic gyre (WAG) and/or coastal jet regime during winter (lower dashed box in Figure 1a). These gyres are the result of the inflow of a jet of AW through the Strait of Gibraltar with an estimated speed of 1 m/s that produces a strong horizontal shear when interacting with the coast [*García-Lafuente et al*., 2000]. The volume transported by the Atlantic jet in the western side of the Alboran Sea subbasin is around 0.8 Sv presenting round year variations. The WAG presents an apparent persistence while the EAG may occasionally disappear [*Viúdez et al*., 1996; *Vargas-Yáñez et al*., 2002]. During autumn, the EAG is well defined and a density front oriented from the NW to the SE is formed (the Almeria-Oran front). This front separates the inflowing "new" AW from the denser out-flowing water masses [*Tintoré et al*., 1988]. The intensity of the EAG modulates the circulation to the east as well as the inflow of AW to the North-Western subbasin. Waters flowing from Alboran to the east form the Algerian Current (AC) which is characterized by its unstable nature presenting meanders of tens of kilometers [*Viúdez et al*., 1998].

3. Data and Methods

3.1. Ocean Currents

[12] Surface currents are obtained from the Western Mediterranean OPerational Model (WMOP) [*Tintoré et al*., 2012]. WMOP provides daily analysis and forecast of currents, temperature, salinity, and sea level anomalies in the WMS. It is based on a regional configuration of the Regional Ocean Modelling System (ROMS) [*Shchepetkin and McWilliams*, 2005], an eddy resolving three dimensional, free-surface, stretched sigma coordinate primitive equation model. The model covers the WMS from 5.8°W to 9.2°E and from 34.9°N to ~44.7°N (Figure 1). The mesh size for the whole domain is 631 × 539 grid points (N_x, N_y) with a resolution of ~1.8 km, allowing a good sampling of the first baroclinic Rossby radius of deformation (about 10–15 km) throughout the whole area [*Send et al*., 1999] and 30 vertical levels. Bathymetry is obtained from a 30″ resolution database [*Smith and Sandwell*, 1997]. The system is daily initialized using temperature, salinity, horizontal velocities, and Sea Surface Height (SSH) from previous restart at $t = -24$ h. At the two lateral open boundaries (south and east), an active, implicit, upstream biased, radiation condition connects the model solution to the surrounding ocean [*Marchesiello et al*., 2001]. Daily Mediterranean ocean Forecasting System (MFS) fields [*Oddo et al*., 2009] are used to infer the thermodynamics at the open boundaries. The atmospheric forcing is included with a bulk formulation for air-sea heat and momentum exchange [*Fairall et al*., 2003], being provided by the HIRLAM model [*Unden et al*., 2002]. HIRLAM is operated by the Spanish Agency of Meteorology, providing a spatial resolution of 5 km and a temporal resolution of 3 h.

3.2. Finite Size Lyapunov Exponents

[13] The surface dynamics is first studied by computing the FSLE from the model velocities obtained at the uppermost model sigma layer. *Galán et al*. [2012] already computed the FSLE of the WMOP surface velocity data in a coastal area testing this approach with the trajectories obtained by Lagrangian drifters transmitting hourly GPS position.

[14] For the FSLE computation, massless particles are advected by the flow being their motion—neglecting vertical movements among different layers—described by

$$\frac{d\phi}{dt} = \frac{v_\phi(\phi,\lambda,t)}{R\cos(\lambda)}, \qquad \frac{d\lambda}{dt} = \frac{v_\lambda(\phi,\lambda,t)}{R}, \tag{1}$$

where ϕ and λ are the longitude and latitude coordinates for each particle respectively, v_ϕ and v_λ the zonal and meridional components of their velocity, t refers to the time, and R is the radius of the Earth (~6.400 km).

[15] The FSLE are measures of dispersion which are obtained by computing the time (T) it takes for two trajectories, initially separated a finite distance (δ_0), to reach a larger final fixed separation (δ_f), i.e.,

$$\Lambda(\phi,\lambda,t,\delta_0,\delta_f) = \frac{1}{\mathrm{T}}\ln\left(\frac{\delta_f}{\delta_0}\right), \tag{2}$$

where Λ is the FSLE for the pair of trajectories having units of inverse of time. FSLE can be computed backwards or forwards in time using at any instant past or future velocity fields, respectively. In this work, we will interpret the FSLE as a scalar measure for mixing and we have computed them backwards in time.

[16] Daily FSLE fields are computed for 3 years from the upper layer model velocities by advecting the massless particles, initially deployed at 12:00 UTC, with an integration time step of dt = 6 h. The advection was limited to a maximum of 30 days, time necessary to reach the desired final distance and even to escape from the study area.

[17] The FSLE depends on the choice of both the initial separation δ_0 and the final separation δ_f [*d'Ovidio et al.*, 2004]. The commencing distance is selected to be the initial model spatial resolution. *Pattantyús-Ábrahám et al.* [2008] suggests that since $\Lambda(x,t,\delta_0,\delta_f)=\frac{1}{T}\log\left(\frac{\delta_f}{\delta_0}\right)$, a decrease of δ_f is equivalent to an increase of δ_0, i.e., to the choice of a coarser resolution, which reflects in fatter filaments. At the end, this is like considering turbulent diffusivity for the Lagrangian dynamics, that is, to include some noise term in the particle trajectories [*Hernández-Carrasco et al.*, 2011]. Here, we have chosen as the final separation (δ_f) a value of 25 km, a distance related with the first internal Rossby radius of deformation—of the order of 10–15 km in the Mediterranean Sea [*Send et al.*, 1999]. Moreover with this final distance, we will filter many of the small-scale features that will introduce noise in the spatiotemporal analysis. As an example, Figure 2 displays snapshots of the FSLE computed for three different days using $\delta_f = 25$ km.

[18] Particles are advected using a fourth-order Runge-Kutta which has a low numerical diffusivity and low computational cost. Virtual particles are initially located over all model grid points being transported by the model velocities. The smallest of the times taken by any of the four neighboring points to reach the final distance δ_f is taken as the value of the FSLE.

[19] The main patterns of variability in the FSLE are obtained through an EOF decomposition [*Emery and Thomson*, 2004]. In short, daily FSLE fields are decomposed in a certain number of eigenvalues and the information decorrelated in two separate space-time components (called modes and amplitudes) as

$$\mathrm{FSLE}(x,y,t) - <\mathrm{FSLE}(x,y,t)> = \sum_{i=1}^{N_t} a_i(t) EOF_i(x,y) \qquad (3)$$

where <,> denotes the temporal average, EOF_i are the eigenmode, and a_i the amplitudes. The eigenvalues of the correlation matrix give the variance explained by their corresponding modes of variability. Figure 3 shows the 3 years averaged FSLE field for the Alboran Sea (left) and for the North-Western subbasin (right) subtracted in the computations of equation (3).

[20] Most of these modes are normally the result of a single episode or just noise being difficult to be interpreted under a physical point of view. But some of the modes (the most statistically significant ones) can be explained in terms of oceanic processes that in the case of the FSLE are related with patterns of surface transport and therefore they can be linked with specific oceanic processes. Original FSLE fields can be reconstructed multiplying all EOF by their corresponding amplitudes, following the equation (3). In fact, since these Lagrangian descriptors provide the instantaneous patterns organizing the flow for a range of

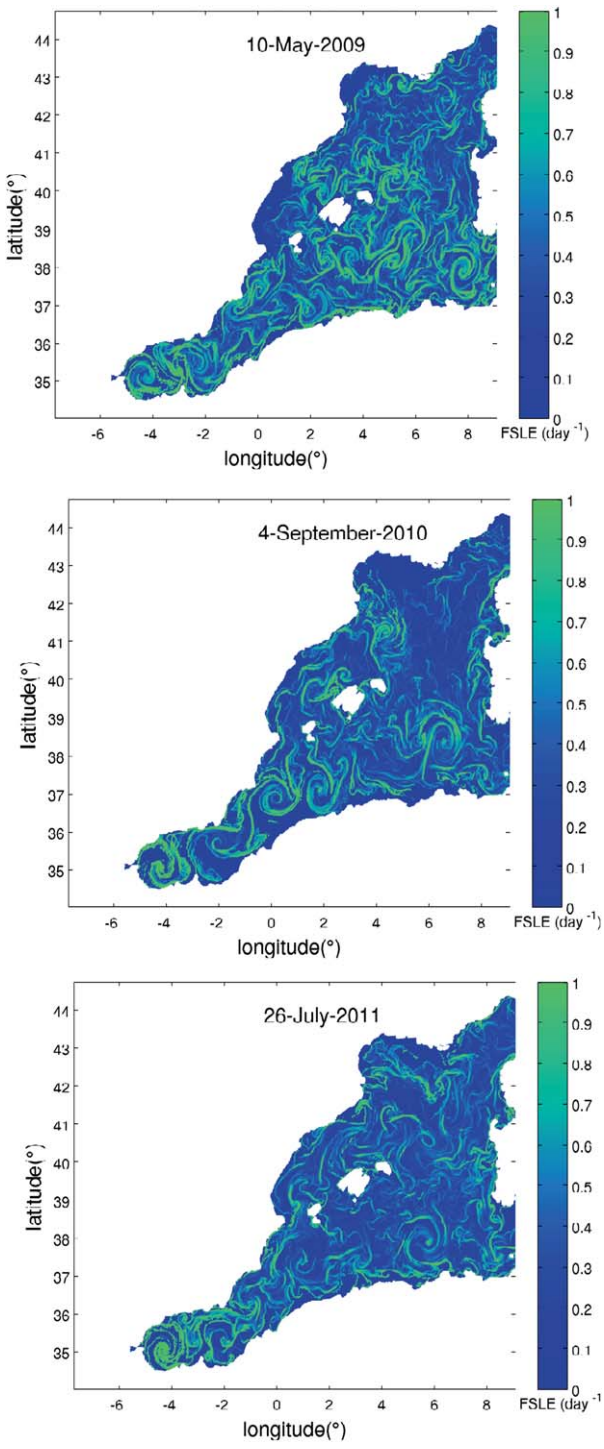

Figure 2. Snapshots of FSLE for (top) 10 May 2009, (center) 4 September 2010, and (bottom) 26 July 2011 for $\delta_f = 25$ km.

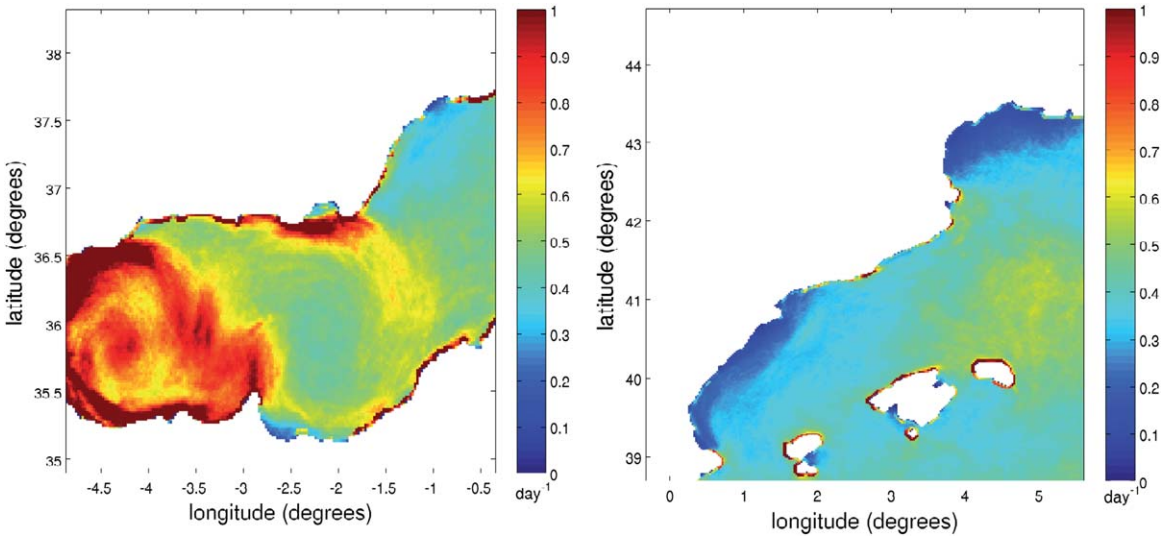

Figure 3. Three year averaged FSLE for the Alboran subbasin (left) and for the North-Western subbasin (right).

spatial scales, the essential processes and main features of (sub)mesoscale circulation can be inferred from them. Since EOF is only a projection of the original data in a new orthogonal base, the interpretation of each mode has to be validated by additional analyses, such as the deployment of Lagrangian particles or the computation of RT, presented below.

3.3. Residence Time

[21] The Residence Time (RT) is a Lagrangian measure that gives information of the rate of water renewal of semi-enclosed areas [*Buffoni et al*., 1996, 1997; *Falco et al*., 2000]. It is defined as the time that a Lagrangian particle stays in a domain before crossing one of its boundaries. The RT can be inferred by advecting backward and forward Lagrangian particles, and computing the time to entry, t_b, and escape, t_f, through a boundary, so that RT = $t_b + t_f$.

4. Results and Discussion

4.1. Spatial and Temporal Variability of the FSLE

[22] EOF analysis was first applied to the FSLE computed over the entire WMS. The first two spatial modes and temporal amplitudes, which represent 18% of the total variability of the FSLE are displayed in Figure 4. The first EOF mode shows an intense activity of the FSLE over the entire WM basin, even more intense where permanent currents are located and on those areas with intense mesoscale activity. Strong features on the two Alboran gyres and the AC are clearly identified. The pathways of eddies detachment are also a clear signature in this EOF mode emerging as the finger-like structures at the mid of the basin (~5°E) that extend northward which indicate this as is a highly dynamical area (Figure 4a). The EOF temporal amplitude presents a seasonal signature (Figure 4b). In addition, the northern area of the North-Western subbasin presents more activity than the southern part which is also in accordance with the literature. This is the result of the strong winds that during the late autumn and in winter affect the area [*Millot*, 1999].

[23] The second EOF presents a similar spatial structure than the first EOF but the seasonal signal is π-out of phase respect to the first EOF (see Figure 4c), for the spatial pattern and Figure 4d for its amplitude. When the spatial mode is multiplied by the temporal amplitude, colors, and signs are compensated providing the first and the second EOF almost the same information. The explained variance of this mode is 5.1% of the total variability.

[24] The explained variance of the third mode (not shown) is around 4% and depicts mainly the area covered by the Liguro-Provenzal current (Northern Current).

[25] Despite that the dominant currents and the large-scale processes such as the AC and the Alboran gyres are well identified in the two most relevant modes of the WMS, they do not allow to assess a detailed description at the regional subbasin scales. Therefore, in the following section, we compute the EOF on both subbasins trying to isolate the dynamics of interest, in particular the main patterns of spatiotemporal variability, and the connectivity between them.

4.1.1. Alboran Sea Subbasin

[26] Spatial modes of the first two EOFs and their corresponding temporal amplitudes are displayed in Figure 5 for the Alboran Sea. The first EOF, explaining around 12% of the total variance, shows the FSLE spatial pattern associated to the WAG and the EAG, as well as the structure of the Atlantic Jet flowing from the EAG (see Figure 5a) into the Algerian subbasin to form the AC. The structure representing the WAG is the most remarkable feature emerging from the FSLE. The main pattern of the EAG is also depicted as well as the Atlantic Jet flowing along the northern coast of Africa toward the east. The temporal amplitude of this EOF (Figure 5b) shows a subseasonal variability. Large values of FSLE (minima in amplitude) are found at the end of autumn/spring. Subseasonal oscillations can be related to the tides, wind stress, or atmospheric pressure

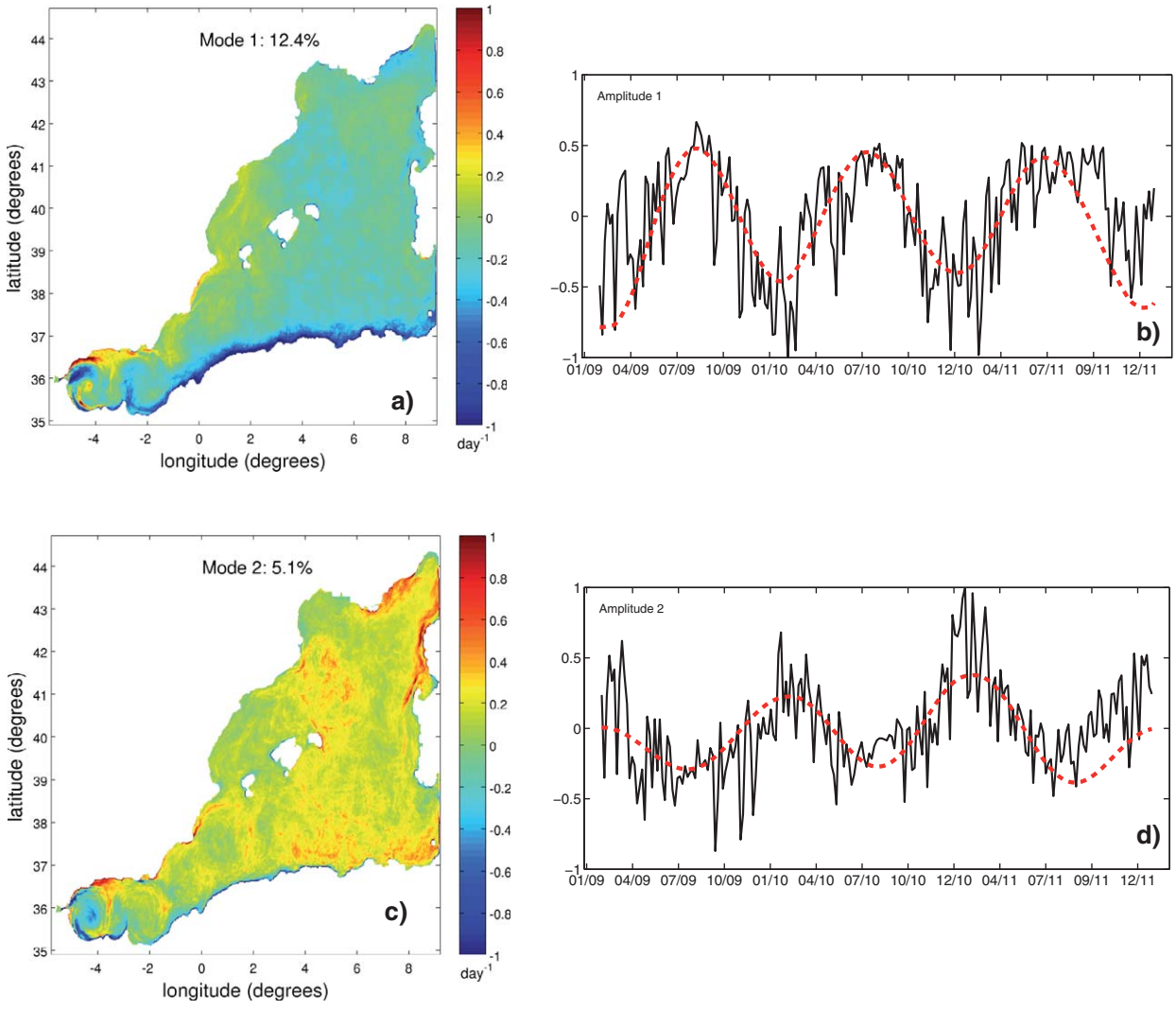

Figure 4. (a) First FSLE-EOF spatial mode, (b) its corresponding temporal amplitude, (c) second FSLE-EOF spatial mode, and (d) its corresponding temporal amplitude for the WM. Dashed red lines over the amplitudes represent the annual component obtained from a Singular Spectrum Analysis.

oscillations, but this is beyond the scope of this study. In fact, the Atlantic Jet undergoes quasi-periodic variations of 10 days period both in its intensity and in its direction [*Perkins et al*., 1990].

[27] The second FSLE-EOF represents 7% of the total variability. The spatial pattern (Figure 5c) shows the modulation of the EAG strengthening/weakening. From the spatial mode and its temporal amplitude (see Figure 5d) we can observe that, at the end of spring of 2010 and 2011, the FSLE of the EAG weakens. It results in the deflection of AW to the north in a structure located parallel to the east Spanish coast toward the Ibiza Channel (this can be seen by reconstructing the corresponding signal from the EOF computation). The EAG is formed generally during the summer disappearing during winter with some exceptions [*Renault et al*., 2012b]. The most remarkable feature of this mode is the abrupt change in amplitude observed at the beginning of summer of 2010 and 2011 (Figure 5d). The reconstructed signal is obtained by multiplying the amplitude with the spatial pattern indicating that these abrupt changes may display the transport of "new" AW to the north as the result of the most likely weakening of the EAG.

[28] With the objective of inferring the spatiotemporal variability of the deflection of AW in this subbasin, we computed the time necessary to travel from the Alboran Sea to the Ibiza Channel (defined as a horizontal target line between Ibiza and the continental coast at 38.7°N, by daily deploying a Lagrangian particle at each model grid point of the Alboran Sea). Those particles arriving to the coast or those crossing a longitudinal threshold located at 1°E were removed after storing their traveling time. The distribution of the time (in days) employed by the particles initially deployed in the Alboran Sea to reach the Ibiza Channel is depicted in Figure 6a. The median time is ∼50 days which gives an averaged velocity 11.5 cm/s if a particle is located

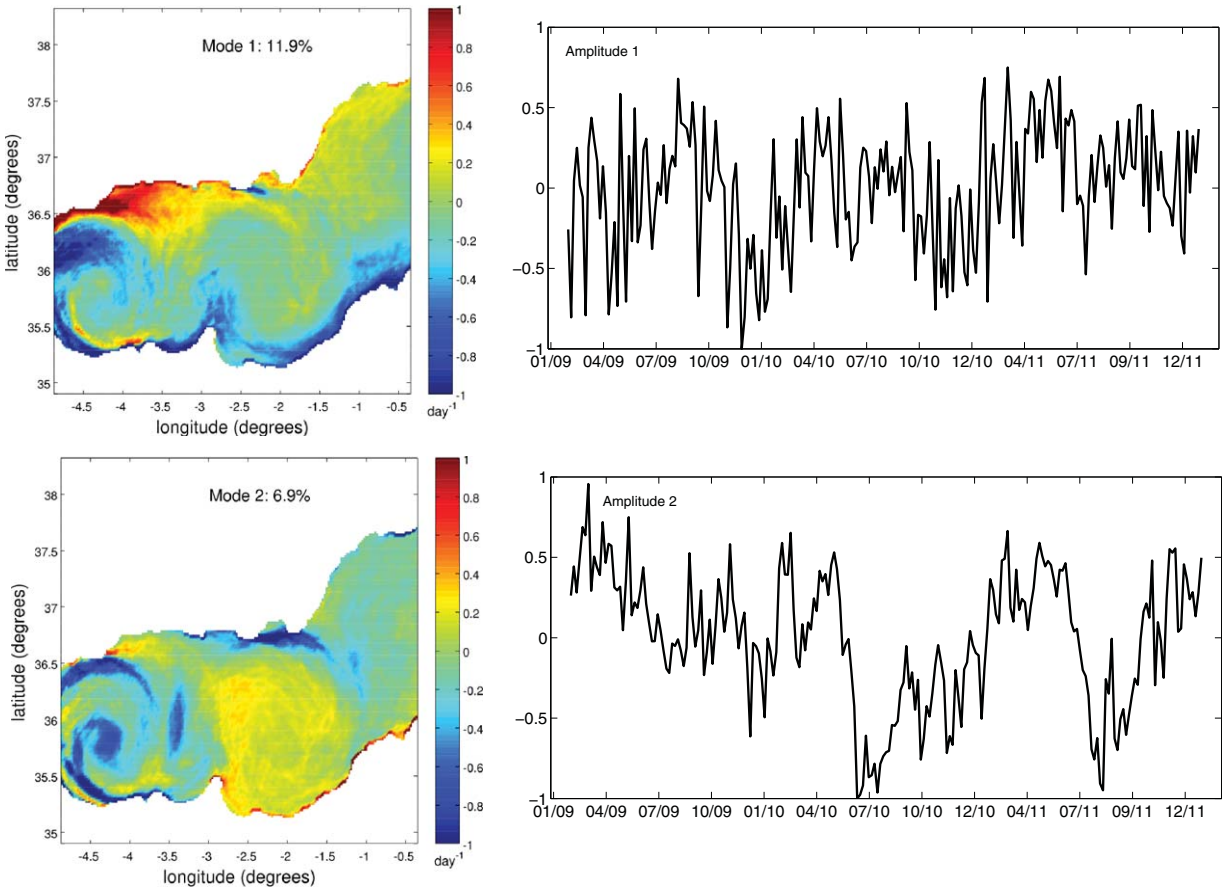

Figure 5. (a) First FSLE-EOF spatial mode, (b) its corresponding temporal amplitude, (c) second FSLE-EOF spatial mode, and (d) its corresponding temporal amplitude for the Alboran Sea subbasin.

at the middle of the Alboran Sea (∼500 km). However, the number of particles crossing the Ibiza Channel is not constant along the year as expected from the variability of the EAG depicted in the second FSLE-EOF mode. The daily fraction (defined as the number of particles crossing the channel divided by the number of particles initially released) of particles is shown in Figure 6b for the 3 years. As seen, the largest number of particles cross the channel during spring/summer when the EAG weakens supporting the hypothesis that this phenomenon drives the intrusion of AW to the North-Western subbasin. Which is in accordance with previous results that have shown that northward transport through the Ibiza Channel is larger during summer and spring, while during winter dominates the transport to the south [*Pinot et al*., 2002; *Heslop et al*., 2012].

4.1.2. North-Western Subbasin

[29] The first FSLE-EOF, which explains 11% of the total variability, shows two different areas in terms of transport (Figure 7a). Between the northern Balearic Islands and the Gulf of Lions there is a highly dynamical zone with large values of FSLE. At the south, there is a less active zone where some small structures arise. The amplitude of this mode has the maxima in summer and more pronounced minima during winter, with a marked seasonal variability, as shown by a Singular Spectrum Analysis of the signal, i.e., a Singular Value Decomposition of the covariance matrix of the temporal amplitude (red line in Figure 7b). The driving mechanisms for the transport represented by this mode are the strong and intense Tramontane and Mistral winds, blowing from the northwestern sectors over the north-Catalan coast during most of the year (see Figure 1). In addition, more intense values during winter are related to stronger winds blowing on the Gulf of Lions through the Rhone Valley. The influence of the wind on this first mode is inferred by performing the coupled Singular Value Decomposition (SVD) between the FSLE and the modulus of the wind stress. In short, both fields are normalized by their standard deviations and combined in the same matrix to compute its covariance. The first two SVD projected on the FSLE fields are displayed in Figure 8. These modes, with a combined covariance of 94% (83.6% the first mode and 10.4% the second mode) indicate that the first FSLE-EOF in the North-Western subbasin is mainly driven by wind. The amplitudes of these two SVD modes are significantly correlated (at the 95% confidence level) with the first FSLE-EOF amplitude at time lag zero (not shown).

[30] The second FSLE-EOF explains about 7% of the total variance (Figures 7c and 7d for the spatial mode and its corresponding amplitude, respectively). The more

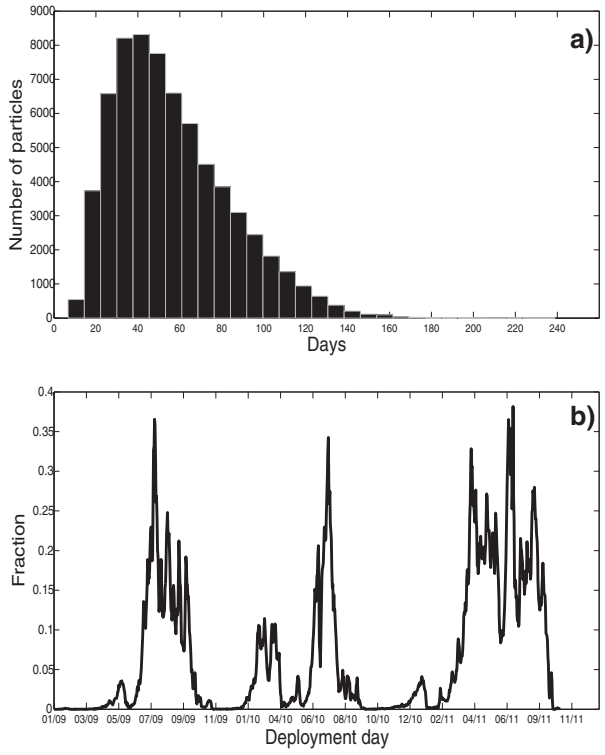

Figure 6. (a) Histogram of the days employed for particles deployed at the Alboran Sea to reach the Ibiza Channel and (b) time series of the fraction of particles arriving to the section. Deployment of particles has been done on each daily field at 12:00 UTC for the 3 years.

homogeneous structure extending all along the coast from the Gulf of Lions to the west side of the Ibiza Channel is the signature of the NC together with the intensification of the winds during autumn. Although NC moves along the slope, without entering in the Gulf of Lions, the spatial signature shows a pattern covering completely the Gulf of Lions as the result of the intense winds mainly during November (see Figure 7d). Previous authors already showed that the maximum intensity of the NC is found during autumn diminishing in winter and spring [*Font et al*., 1995]. The high values of FSLE in the western and southern part of the basin are associated with the movement of eddies and other energetic features.

[31] The third FSLE-EOF explains around 3% of the total variability and, its most remarkable feature is what seems to be a structure that appears as a tongue along the southern part of the Spanish coast (Figure 7e), displaying high frequency variability (Figure 7f). This structure that crosses the Ibiza Channel toward the North-Western subbasin is the inflow of AW from the Alboran Sea and is likely related with the deflection of AW when the EAG is weak or has disappeared. Therefore, we expect this amplitude to be related with the amplitude of the second FSLE-EOF mode of the Alboran Sea which was identified as the one explaining the deflection of AW. The cross correlation between these amplitudes is presented in Figure 9. A significant correlation is obtained with a time lag of 40–50 days (>0.15) coincident with the median time for a particle located at the Alboran Sea to reach the Ibiza Channel.

4.1.3. Residence Time

[32] In this section, we use the Residence Time concept to summarize briefly the features and processes explained previously. For the 3 years analyzed, Figure 10 shows the time series of the RT averaged for all of each subbasin. As seen, there is a marked seasonality in the RT at both basins. In the Alboran sea, minima values are in summer while in the North-Western subbasin they are in autumn, when the strong low pressure systems affect the area. Selected snapshots of the RT computed for the Alboran Sea and the North-Western subbasins together with the corresponding SST fields are shown in Figures 11 and 12, see the supporting information for the complete simulation. On 28 November 2011, the two Alboran gyres are clearly identified from both the RT and the SST as seen in Figures 11a and 11b with an eddy-like structure in the RT representing the WAG with low values of the RT as the renewal of waters due to the inflow of waters through the Strait of Gibraltar, and the EAG with higher values of RT where particles remain longer time. The displacement of the WAG, as explained by *Viúdez et al*. [1998], and the weakening of the EAG are shown in Figures 11c and 11d for 17 May 2011. In this configuration, the EAG is not totally formed appearing as a small (or third eddy) located near the Algerian coast. This situation breaks partially the anticyclonic circulation deflecting part of the AW of the Alboran subbasin to the north reaching the Ibiza Channel 7 weeks later. This is the configuration explained by the second EOF of the Lyapunov exponent (Figure 5c). The RT and SST for 7 October 2011 (Figures 12e and 12f) show the typical configuration of the Almeria-Oran front that separates the new waters from the old ones.

[33] The structure in the North-Western subbasin for 30 October 2009 (Figures 12a and 12b) display the inflow of AW through the Ibiza Channel. It can be observed the cyclonic retroflexion of the NC at the southern part of the domain. Contrarily, on 6 March 2011 Figures 12c and 12d, the AW does not cross the Ibiza Channel and the NC is flowing to the south, eventually arriving to the Alboran subbasin. When these water masses arrive to the Alboran subbasin if the EAG is developed (as depicted in Figures 11e and 11f) these waters are blocked by the Almeria-Oran front. Finally, Figures 12e and 12f show a typical winter situation with a strong dynamical activity in the area of the Gulf of Lions where values of RT are extremely small due to the strong winds during 29 September 2011. The low values of RT are a good indication of the formation of meso and submesoscale processes such as the density instabilities, fronts, filaments, and eddies depicted in Figure 12f.

5. Conclusions

[34] In this work, we use Lagrangian descriptors (FSLE, residence times, particle trajectories) to analyze the main characteristics of the surface flow of the Western Mediterranean Sea. To achieve this we have departed from the velocity fields of an eddy resolving primitive equation numerical model. The FSLE has been already shown to be a valuable tool to study transport and dispersion processes. Due to the large spatial and temporal variability of the FSLE the EOF technique has been used to extract the main

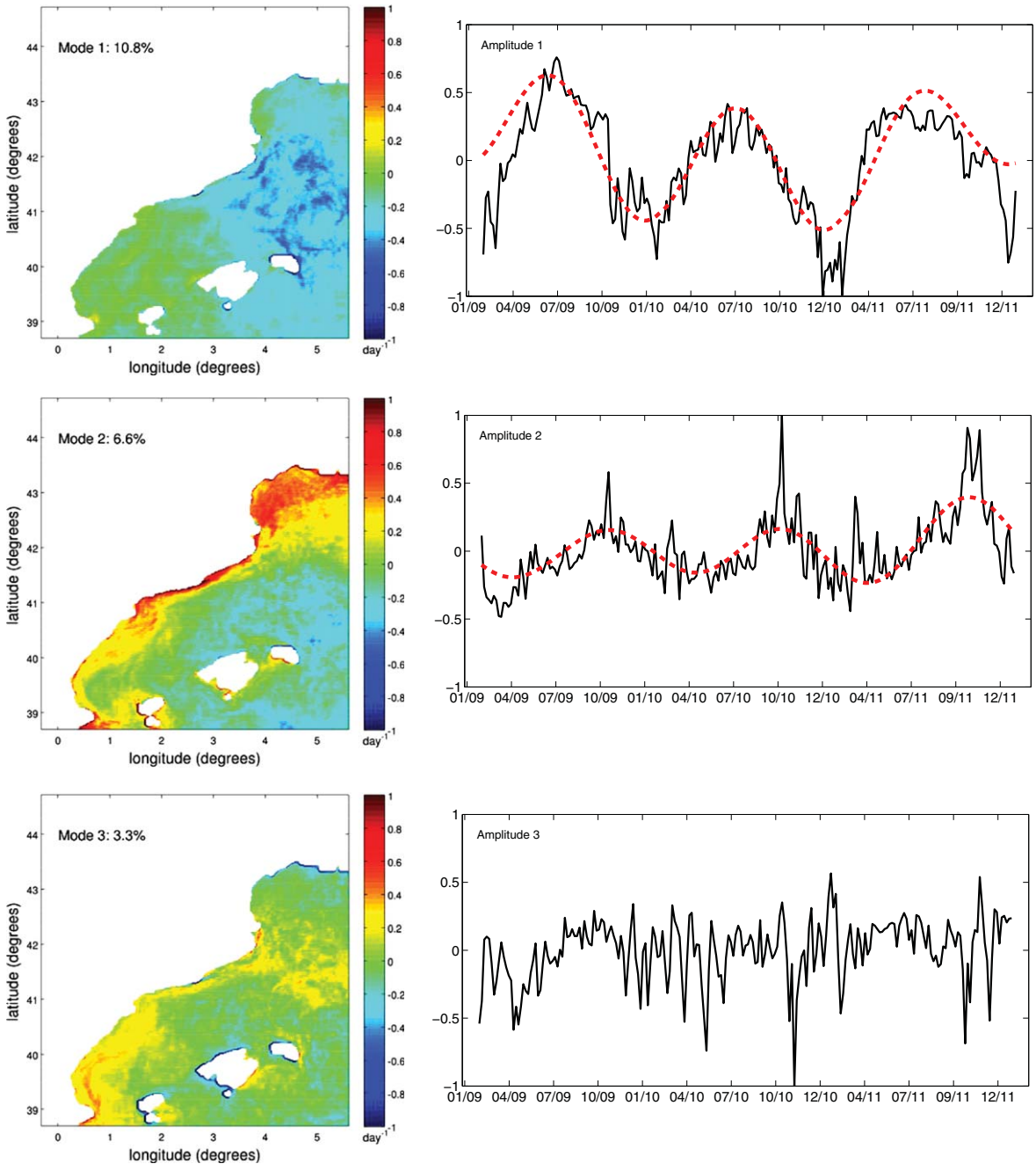

Figure 7. (a) First FSLE-EOF spatial mode, (b) its corresponding temporal amplitude; (c) second FSLE-EOF spatial mode, (d) its corresponding temporal amplitude, (e) third FSLE-EOF spatial mode, and (f) its corresponding temporal amplitude for the North-Western subbasin. Dashed red lines over the first and second amplitudes represent the annual component obtained from a Singular Spectrum decomposition.

patterns of variability of two crucial subbasins of the WMS, the Alboran Sea, and the North-Western. The most representative (in terms of explained variance) modes of variability of both subbasins are analyzed.

[35] The main pattern of circulation in the Alboran Sea, described by the WAG and the quasi-permanent EAG, is represented by the first EOF of the FSLE which contains ~12% of the total variability of the surface transport, displaying the more frequent disposition of the gyres as well as the pattern of the AC. The weakening of the EAG and the consequent disappearance of the Almeria-Oran front, explained by the second FSLE-EOF which is a 7% of the variability of the surface transport. This situation is associated with the deflection of "new" AW to the North. The median time, according to the histogram, took by particles located at the Alboran Sea surface to reach the Ibiza Channel is of ~50 days being the transport more efficient during the mid-summer.

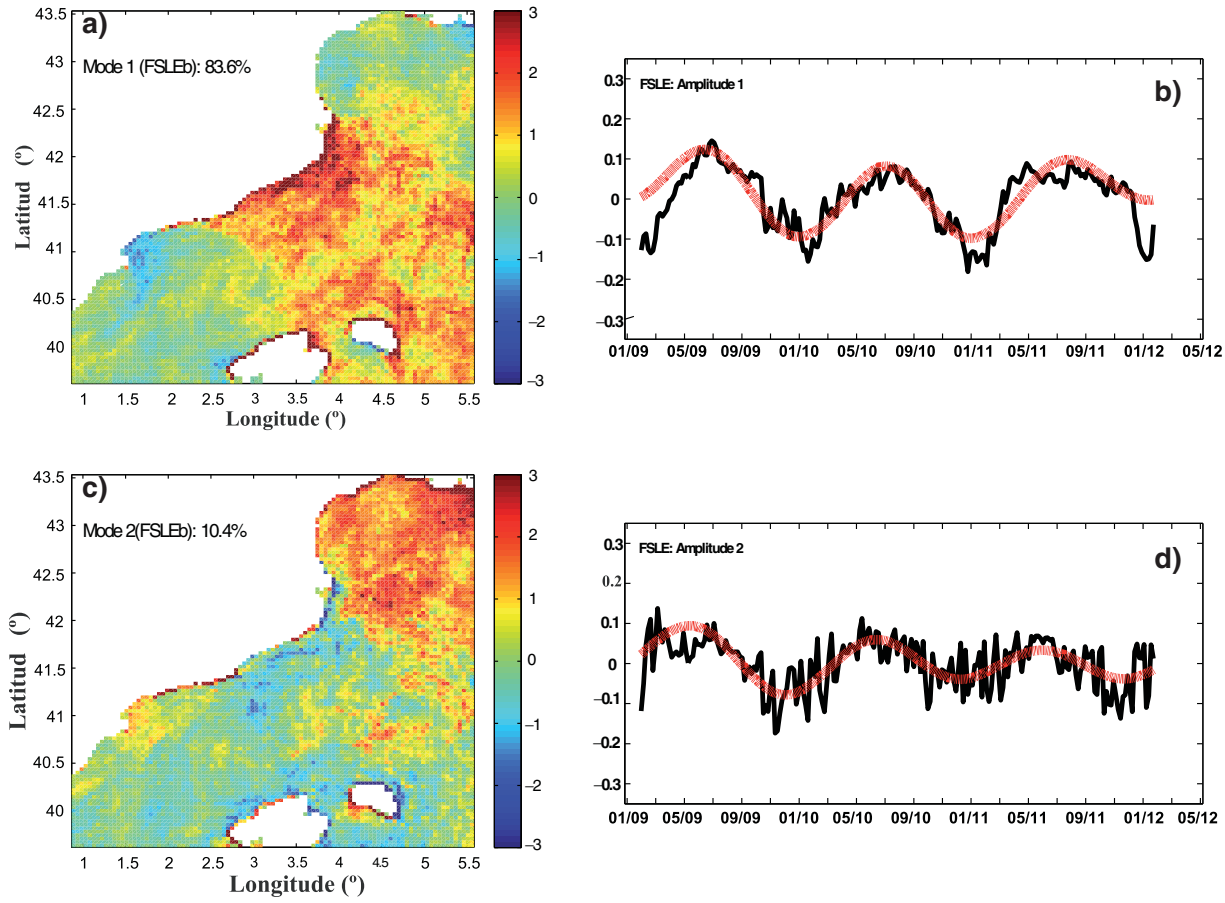

Figure 8. (a) First coupled FSLE-EOF and wind SVD spatial mode, (b) its corresponding temporal amplitude, (c) second coupled FSLE-EOF and wind SVD spatial mode, and (d) its corresponding temporal amplitude. Dashed red lines over the amplitudes represent the annual component obtained from a Singular Spectrum Analysis.

[36] The North-Western subbasin main patterns of variability have been identified by the three first FSLE-EOF modes. The first mode, representing 11% of the total variability is related with the wind forcing resulting in two different areas in terms of transport: the northern part, very

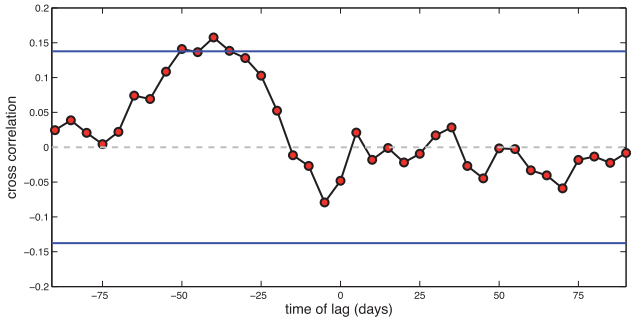

Figure 9. Cross correlation between the temporal amplitude of the second FSLE-EOF of Alboran Sea subbasin and the amplitude of the third FSLE-EOF of the North-Western subbasin. Blue lines are the 95% confidence interval for the autocorrelations of an independent and identically distributed random variable process.

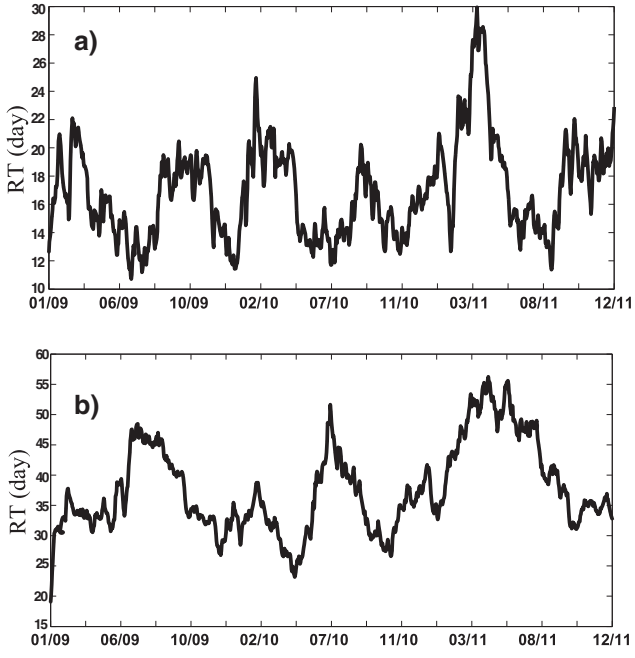

Figure 10. Time Series of RT daily averaged by subbasins: (a) Alboran Sea and (b) North-Western.

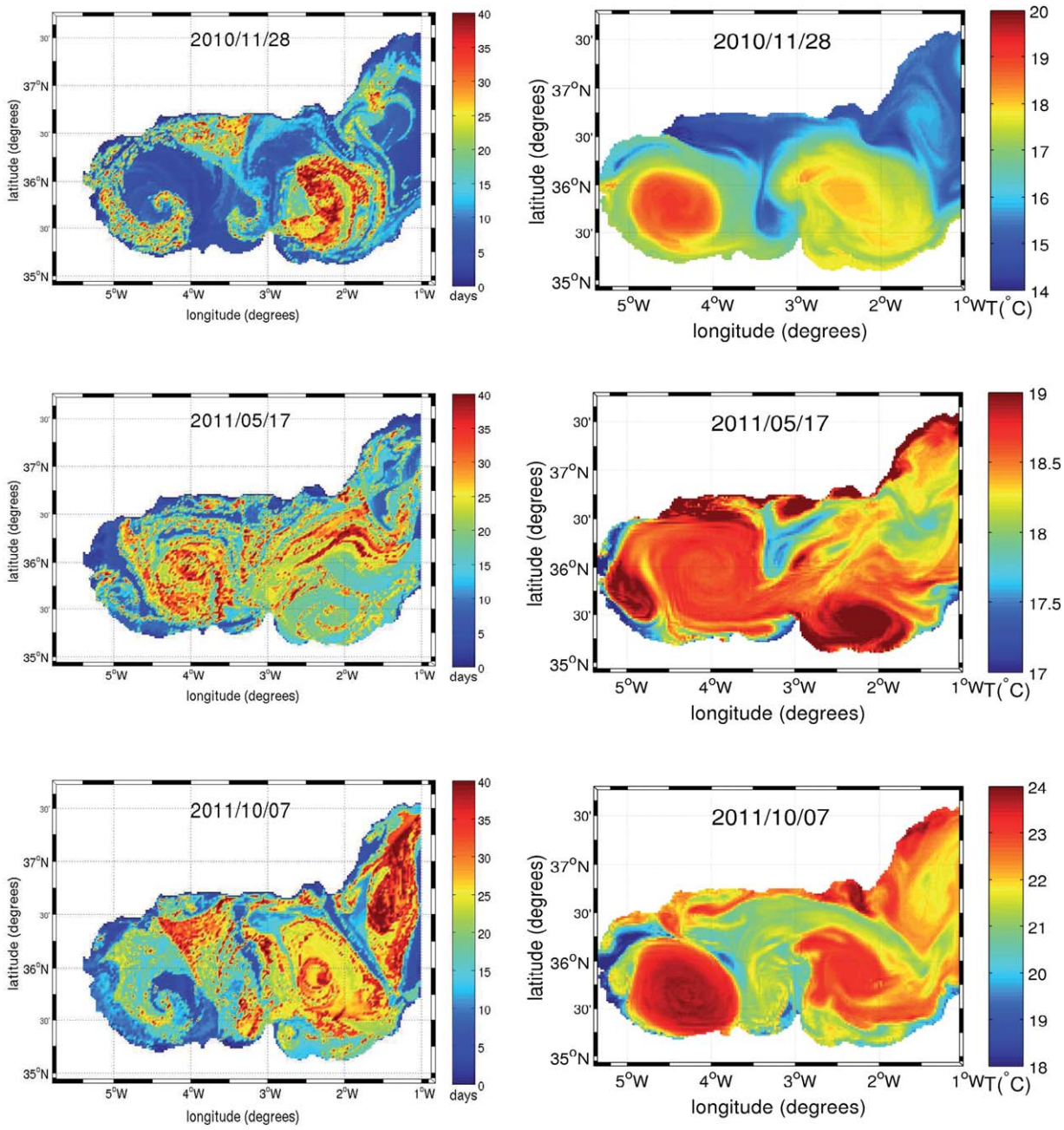

Figure 11. Residence time (left) and SST (right) snapshot for selected days (units are days and °C, respectively), computed for the Alboran Sea subbasin.

active, and the southern part, much less active. The second EOF is related with the coastal NC and represents 7% of the surface transport. A relevant feature is a well-defined shelf-bounded pattern that flows all over the coast from the Ligurian subbasin to the southern edge of the Catalan Sea. Finally, the third EOF describes the intrusion of AW in the North-Western subbasin as the result of the weakening of the EAG explained by the second EOF mode of the Alboran Sea. A cross-correlation analysis shows that both phenomena are correlated in the 95% statistical confidence level with a time lag of 40–50 days, which has been shown to be approximately the median time it takes for a particle to travel from the Alboran Sea subbasin to the Ibiza Channel.

[37] In addition, we have used the Residence Time as a Lagrangian descriptor to visualize the main features obtained by the FSLE-EOF decomposition. We show that the global aspect of the flow can be studied by the FSLE and when combined with statistical techniques such as the EOFs are a complementary tool to the traditional Eulerian descriptors. In order to get a more understandable knowledge of the presented approach we suggest to use both, numerical, and observational data from altimetry, to widen the study to the interannual scale. Finally, this work is

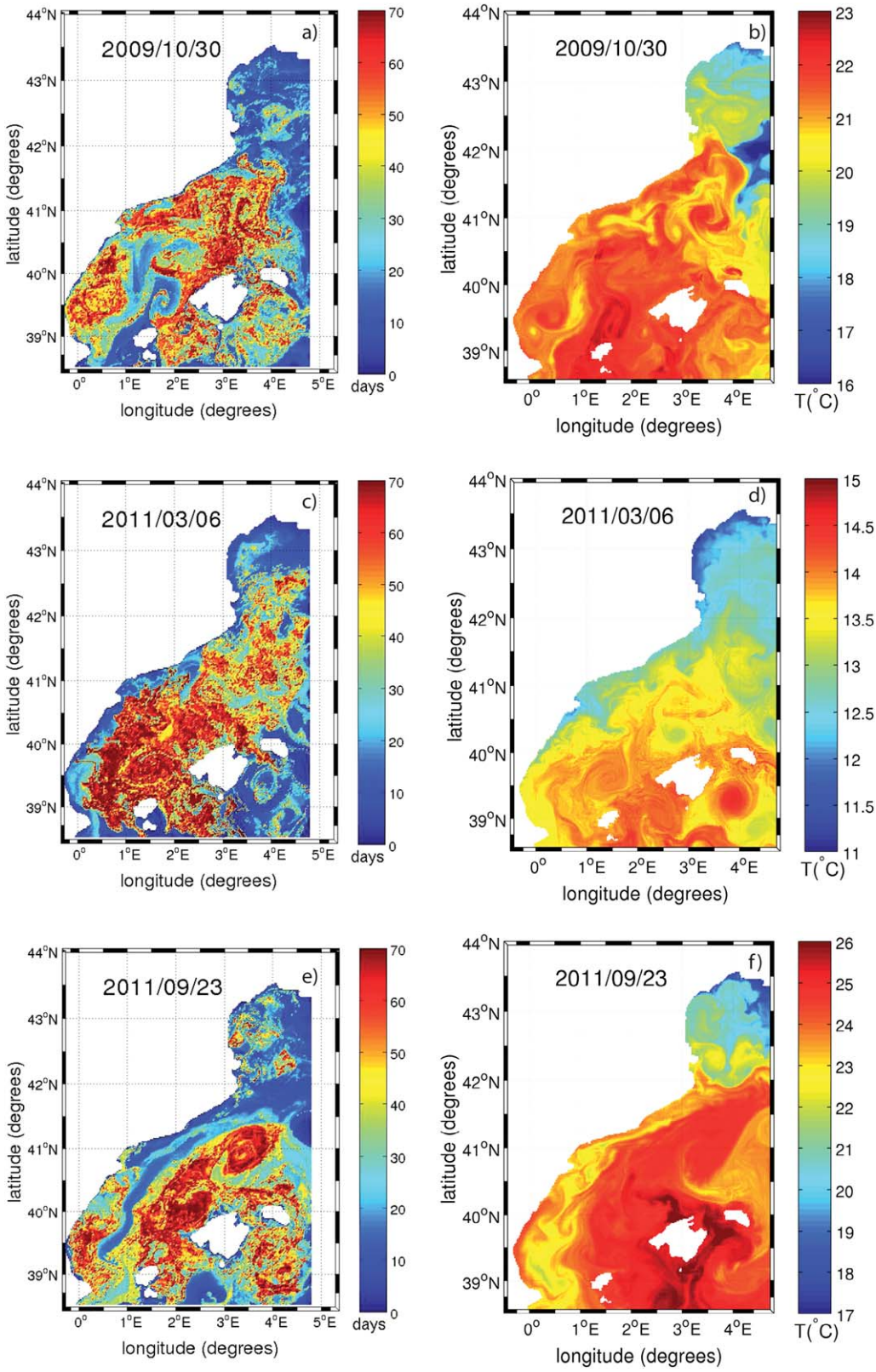

Figure 12. Residence time (left) and SST (right) snapshots for selected days (units are days and °C, respectively), computed for the North-Western subbasin.

restricted to the surface circulation but some effort should be devoted to reproduce these analyses for the 3D circulation, in order to track with more details the main patterns of water masses transport.

[38] **Acknowledgments.** J.M.S. is supported by the PhD CSIC-JAE program cofunded by the European Social Fund (ESF). G.S. is supported by the Spanish government through the "Ramón y Cajal" program. Authors would like to thank financial support from MED Projects TOSCA (G-MED09-425) and MEDESS-4MS funded by FEDER Funds. The authors also thank financial support from MICINN through Project 289 445 CGL2011-22964. Authors strongly thank the Government of the Balearic Islands and FEDER through the "Grups Competitius" program. C.L. acknowledges Spanish MINECO and FEDER through project ESCOLA (CTM2012-39025-C02-01). This work was partly performed while A.O. was a visiting scientist at the Mediterranean Institute of Oceanography at the Université du Sud-Toulon-Var through a MECD grant. Support from SOCIB modeling and Engineering facilities are greatly acknowledged.

References

André, G., P. Garreau, V. Vernier, and P. Fraunié (2005), Modelled variability of the sea surface circulation in the North-western Mediterranean Sea and in the Gulf of Lions, *Ocean Dyn.*, *55*, 294–308, doi:10.1007/s10236-005-0013-6.

Artale, V., G. Boffetta, A. Celani, M. Cencini, and A. Vulpiani (1997), Dispersion of passive tracers in closed basins: Beyond the diffusion coefficient, *Phys. Fluids*, *9*(11), 3162–3171.

Aurell, E., G. Bofetta, A. Crisanti, G. Paladin, and A. Vulpiani (1997), Predictability in the large: An extension of the concept of Lyapunov exponent, *J. Phys. A Math. Gen.*, *30*(1), 1–26, doi:10.1088/0305–4470/30/1/003.

Bergamasco, A., and P. Malanotte-Rizzoli (2010), The circulation of the Mediterranean Sea: A historical review of experimental investigations, *Adv. Oceanogr. Limnol.*, *1*(1), 11–28, doi:10.1080/19475721.2010.491656.

Boffetta, G., G. Lacorata, G. Redaelli, and A. Vulpiani (2001), Detecting barriers to transport: A review of different techniques, *Physica D*, *159*, 58–70.

Buffoni, G., A. Cappelletti, and E. Cupini (1996), Advection-diffusion processes and residence times in semi-enclosed marine basins, *Int. J. Numer. Methods Fluids*, *22*, 1–23.

Buffoni, G., P. Falco, A. Griffa, and E. Zambianchi (1997), Dispersion processes and residence times in a semi-enclosed basin with recirculating gyres: An application to the Tyrrhenian Sea, *J. Geophys. Res.*, *102*(C8), 18,699–18,713, doi:10.1016/j.jmarsys.2007.02.010.

d'Ovidio, I., V. Fernandez, E. Hernandez-Garcia, and C. Lopez (2004), Mixing structures in the Mediterranean Sea from finite-size Lyapunov exponents, *Geophys. Res. Lett.*, *31*, L17203, doi:10.1029/2004GL020328.

d'Ovidio, I., J. Isern-Fontanet, C. Lopez, E. Hernandez-Garcia, and E. Garcia-Ladona (2009), Comparison between Eulerian diagnostics and finite-size Lyapunov exponents computed from altimetry in the Algerian basin, *Deep Sea Res., Part I*, *56*, 15–31, doi:10.1016/j.dsr.2008.07.014.

Emery, W.-J., and R.-E. Thomson (2004), *Data Analysis Methods in Physical Oceanography*, chap. 4, Elsevier, Netherlands.

Estournel, C., X. Durreu de Madron, P. Marsaleix, F. Auclair, C. Julliand, and R. Vehil (2003), Observation and modelling of winter coastal oceanic circulation in the Gulf of Lions under wind conditions influenced by the continental orography (FETCH experiment), *J. Geophys. Res.*, *108*, 8059, doi:10.1029/2001JC000825.

Fairall, C.-W., E.-F. Bradley, J.-E. Hare, A.-A. Grachev, and J.-B. Edson (2003), Bulk parameterization of air-sea fluxes: Updates and verification for the COARE Algorithm, *J. Phys. Oceanogr.*, *16*, 571–591.

Falco, P., A. Griffa, and P.-M. Poulain (2000), Transport properties in the Adriatic Sea as deduced from drifter data, *J. Phys. Oceanogr.*, *30*(8), 2055–2071.

Font, J., J. Salat, and J. Tintoré (1988), Permanent features of the circulation in the Catalan Sea, *Oceanol. Acta*, *S-9*, 51–57.

Font, J., E. García-Ladona, and E. Górriz (1995), The seasonality of mesoscale motion in the Northern Current of the western Mediterranean: several years of evidence, *Oceanol. Acta*, *18*(2), 207–219.

Galán, A., A. Orfila, G. Simarro, I. Hernández-Carrasco, and C. López (2012), Wave mixing rise inferred from Lyapunov exponents, *Environ. Fluid Mech.*, *56*(4), 686–703, doi:10.1007/s10652-012-9238-3.

García-Lafuente, J., J.-M. Vargas, F. Plaza, T. Sarhan, J. Candela, and B. Bascheck (2000), Circulation of water masses through the Ibiza Channel, *J. Geophys. Res.*, *105*(C6), 14,197–14,213.

Haller, G., and G. Yuan (2000), Lagrangian coherent structures and mixing in two-dimensional turbulence, *Physica D*, *147*, 352–370.

Haza, A.-C., T.-M. Özgökmen, A. Griffa, A. Molcard, P.-M. Poulain, and G. Peggion (2010), Transport properties in small-scale coastal flows: Relative dispersion from VHF radar measurements in the gulf of la spezia, *Ocean Dyn.*, *60*, 861–882, doi:10.1007/s10236-010-0301-7.

Hernández-Carrasco, I., C. López, E. Hernández-García, and A. Turiel (2011), How reliable are finite-size Lyapunov exponents for the assessment of ocean dynamics?, *Ocean Modell.*, *36*(208–218), doi:10.1016/j.ocemod.2010.12.006.

Heslop, E., S. Ruíz, J. Allen, J.-L. López-Jurado, L. Renault, and J. Tintoré (2012), Autonomous underwater gliders monitoring variability at choke points in our ocean system: A case study in the Western Mediterranean Sea, *Geophys. Res. Lett.*, *39*, L20604, doi:10.1029/2012GL053717.

Iudicone, D., G. Lacorata, V. Rupolo, R. Santoleri, and A. Vulpiani (2002), Sensitivity of numerical tracer trajectories to uncertainties in OGCM velocity fields, *Ocean Modell.*, *4*, 313–325.

Jansà, A. (1987), Distribution of the Mistral: A satellite observation, *Meteorol. Atmos. Phys.*, *36*, 201–214.

Joseph, B., and B. Legras (2002), Relation between kinematic boundaries, stirring, and barriers for the Antarctic polar vortex, *J. Atmos. Sci.*, *59*, 1198–1212.

La Violette, P.-E., J. Tintoré, and J. Font (1990), The surface circulation of the Balearic sea, *J. Geophys. Res.*, *95*(C2), 1559–1568.

Lapeyre, G. (2002), Characterization of finite-time Lyapunov exponents and vectors in two-dimensional turbulence, *Chaos*, *12*(3), 688–698, doi:10.1063/1.1499395.

Lehahn, Y., F. d'Ovidio, M. Lévy, Y. Amitai, and E. Heifetz (2011), Long range transport of a quasi isolated chlorophyll patch by an Agulhas ring, *Geophys. Res. Lett.*, *38*, L16610 doi:10.1029/2011GL048588.

Lekien, F., C. Coulliette, A.-J. Mariano, E.-H. Ryan, L. Shay, G. Haller, and J. Marsden (2005), Pollution release tied to invariant manifolds: *A case study for the coast of Florida, Physica D*, *210*, 1–20, doi:10.1016/j.physd.2005.06.023.

Mancho, A.-M., D. Small, and S. Wiggins (2006), A tutorial on dynamical systems concepts applied to Lagrangian transport in oceanic flows defined as finite time data sets: Theoretical and computational issues, *Phys. Rep.*, *437*, 55–124, doi:10.1016/j.physrep.2006.09.005.

Marchesiello, P.-J.-C., J.-C. McWilliams, and A. Shchepetkin (2001), Open boundary conditions for long-term integration of regional oceanic models, *Ocean Modell.*, *3*(1–2), 1–20, doi:10.1016/S1463–5003(00)00013-5.

Mariano, A.-J., A. Griffa, T.-M. Özgökmen, and E. Zambianchi (2002), Lagrangian analysis and predictability of coastal and ocean dynamics, *Journal of Atmospheric and Oceanic Technology*, *19*(7), 1114–1126.

Millot, C. (1999), Circulation in the Western Mediterranean sea, *J. Mar. Syst.*, *20*, 423–442.

Molcard, A., A.-C. Poje, and T.-M. Özgökmen (2006), Directed drifter launch strategies for Lagrangian data assimilation using hyperbolic trajectories, *Ocean Modell.*, *12*, 268–289, doi:10.1016/j.ocemod.2005.06.00410.1007/s00477-011-0548-7.

Oddo, P., M. Adani, N. P.C. Fratianni, M. Tonani, and D. Pettenuzzo (2009), A nested Atlantic-Mediterranean Sea general circulation model for operational forecasting, *Ocean Sci. Discuss.*, *6*(2), 1093–1127, doi:10.5194/osd-6–1093-2009.

Olascoaga, M., and G. Haller (2012), Forecasting sudden changes in environmental pollution patterns, *Proc. Natl. Acad. Sci. U. S. A.*, *109*(13), 4738–4743, doi:10.1073/pnas.1118574109.

Özgökmen, T.-M., A. Griffa, A.-J. Mariano, and L.-I. Piterbarg (2000), On the predictability of Lagrangian trajectories in the ocean, *J. Atmos. Oceanic Technol.*, *56*, 15–31, doi:10.1016/j.dsr.2008.07.014.

Pattantyús-Ábrahám, M., T. Tel, T. Krámer, and J. Józsa (2008), Mixing properties of a shallow basin due to wind induced chaotic flow, *Adv. Water Resour.*, *31*(3), 525–534, doi:10.1016/j.advwatres.2007.11.001.

Perkins, H., T. Kinder, and P.-E. La Violette (1990), The Atlantic inflow in the Western Alboran Sea, *J. Phys. Oceanogr.*, *20*, 242–263.

Pinot, J.-M., J.-L. López-Jurado, and M. Riera (2002), The Canales experiment (1996–1998). Interannual, seasonal and mesoscale variability of the circulation in the Balearic Channels, *Prog. Oceanogr.*, *55*, 335–370.

Poulain, P.-M., M. Menna, and E. Mauri (2012), Surface geostrophic circulation of the Mediterranean Sea derived from drifter and satellite altimeter data, *J. Phys. Oceanogr.*, *42*, 973–990, doi:10.1175/JPO-D-11–0159.1.

Renault, L., J. Chiggiato, J.-C. Warner, M. Gomez, G. Vizoso, and J. Tintoré (2012a), Coupled atmosphere-ocean-wave simulations of a storm event over the Gulf of Lion and Balearic Sea, *J. Geophys. Res.*, *117*, C09019, doi:10.1029/2012JC007924.

Renault, L., T. Orguz, A. Pascual, G. Vizoso, and J. Tintoré (2012b), Surface circulation in the Alboran Sea (Western Mediterranean) inferred from remotely sensed data, *J. Geophys. Res.*, *117*, C08009, 11, doi: 10.1029/2011JC007659.

Roussenov, V., E. Stanev, V. Artale, and N. Pinardi (1995), A seasonal model of the Mediterranean Sea general circulation, *J. Geophys. Res.*, *100*(C7), 13,515–13,538.

Rubio, A., V. Taillandier, and P. Garreau (2009), Reconstruction of the Mediterranean northern current variability and associated cross-shelf transport in the gulf of lions from satellite-tracked drifters and model outputs, *J. Mar. Syst.*, *78*, 63–78, doi:10.1016/j.jmarsys.2009.01.011.

Send, U., J. Font, G. Krahmann, C. Millot, M. Rhein, and J. Tintore (1999), Recent advances in observing the physical oceanography of the Western Mediterranean, *Prog. Oceanogr.*, *44*, 37–64.

Shadden, S., F. Lekien, and J. Marsden (2005), Definition and properties of Lagrangian coherent structures from finite-time Lyapunov exponents in two-dimensional aperiodic flows, *Physica D*, *212*, 271–304, doi: 10.1016/j.physd.2005.10.007.

Shchepetkin, A., and J. McWilliams (2005), The regional ocean modeling system (ROMS): A split-explicit, free-surface, topography-following-coordinate oceanic model, *Ocean Modell.*, *9*(4), 1577–1585, doi: 10.1016/j.ocemod.2004.08.002.

Smith, W., and D. Sandwell (1997), Global seafloor topography from satellite altimetry and ship depth soundings, *Science*, *277*, 1957–1962.

Tew Kai, E., V. Rossi, J. Sudre, H. Weimerskich, C. Lopez, E. Hernández-García, F. Marsac, and V. Garçon (2009), Top marine predators track Lagrangian coherent structures, *Proc. Natl. Acad. Sci. U. S. A.*, *106*(20), 8245–8250, doi:10.1073/pnas.0811034106.

Tintoré, J., P. La Violette, I. Blade, and A. Cruzado (1988), A study of an intense density frontin the eastern Alboran sea, *J. Phys. Oceanogr.*, *18*, 1384–1397.

Tintoré, J., et al. (2012), SOCIB the impact of new marine infrastructures and forecasting the Mediterranean Sea, in *Designing Med-SHIPS: A Program for Repeated Oceanographic Surveys*, *N. 43 CIESM Workshops Monographs*, edited by F. Briand, pp. 99–118, CIESM, Monaco.

Unden, P., et al. (2002), HIRLAM-5 Scientific Documentation. HIRLAM-5 project.

Vargas-Yáñez, M., T. Ramírez, D. Cortés, M. Sebatián, and F. Plaza (2002), Warming trends in the continental shelf of Malaga Bay (Alboran Sea), *Geophys. Res. Lett.*, *29*(22), 2082, doi:10.1029/2002GL015306.

Viúdez, A., J. Tintoré, and R. Haney (1996), Circulation in the Alboran Sea as determined by the quasi-synoptic hydrographic observations. Part I: Three-dimensional structure of the two anticyclonic Gires, *J. Phys. Oceanogr.*, *26*, 684–705.

Viúdez, A., J. Pinot, and R. Haney (1998), On the upper layer circulation in the Alboran Sea, *J. Geophys. Res.*, *103*(C10), 21,653–21,666.

Wang, D., M. Vieira, J. Salat, J. Tintoré, and P. La Violette (1988), A shelf/slope frontal filament off northeast Spanish coast, *J. Mar. Res.*, *46*(2), 321–332.